RI 8551

Bureau of Mines Report of Investigations/1981

Structure Study of a CF_2Br_2-Inhibited Methane Flame

Effect of CF_2Br_2 on Composition, Net Reaction Rates, and Rate Coefficients

By J. F. Papp, C. P. Lazzara, and J. C. Biordi

UNITED STATES DEPARTMENT OF THE INTERIOR

Report of Investigations 8551

Structure Study of a CF_2Br_2-Inhibited Methane Flame

Effect of CF_2Br_2 on Composition, Net Reaction Rates, and Rate Coefficients

By J. F. Papp, C. P. Lazzara, and J. C. Biordi

UNITED STATES DEPARTMENT OF THE INTERIOR
James G. Watt, Secretary
BUREAU OF MINES

This publication has been cataloged as follows:

Papp, John F

Structure study of a CF_2Br_2-inhibited methane flame. Effect of CF_2Br_2 on composition, net reaction rates, and rate coefficients.

(Report of investigations - Bureau of Mines ; 8551)
Bibliography: p. 29-32.
Supt. of Docs. I 28.23:8551.

1. Flame. 2. Methane. 3. Dibromodifluoromethane. 4. Chemical inhibitors. I. Lazzara, Charles P., joint author. II. Biordi, Joan C., joint author. III. Title. IV. Series: United States. Bureau of Mines. Report of investigations ; 8551.

TN23.U43 [QD516] 622s [628.9'223] 80-606846 AACR1

CONTENTS

ILLUSTRATIONS

ILLUSTRATIONS--Continued

TABLES

STRUCTURE STUDY OF A CF_2Br_2-INHIBITED METHANE FLAME

Effect of CF_2Br_2 on Composition, Net Reaction Rates, and Rate Coefficients

by

J. F. Papp,[1] C. P. Lazzara,[2] and J. C. Biordi[3]

ABSTRACT

The microstructures of a CF_2Br_2-inhibited methane flame and its uninhibited analog have been determined using molecular beam-mass spectrometry. The slightly lean flames were stabilized on a cooled porous plug burner at reduced pressure. Composition profiles of stable, intermediate, and radical species and temperature profiles were obtained. Comparisons of the uninhibited and inhibited flame profiles revealed the following inhibition effects; a shift of the primary reaction zone to higher temperatures, a higher maximum flame temperature, an increase in the CH_3 concentration, and a reduction in the H_2CO, H, O, and OH concentrations. Kinetic analyses of the data yielded rate coefficients at flame temperatures for the reactions $H + CH_4 \rightarrow CH_3 + H_2$, $H + O_2 \rightarrow OH + O$, $CO + OH \rightarrow CO_2 + H$, and $CH_3 + O \rightarrow H_2CO + H$. CF_2Br_2 is judged to decay by thermal decomposition and abstraction reactions.

INTRODUCTION

Chemical flame inhibitors act by interfering with the normal chemical reaction paths of flame propagation. This report is one of a series documenting an effort to provide the data required to understand the mechanisms by which flame inhibitors operate at the molecular level.

In preceding papers the microstructure, kinetics, and mechanisms have been reported for methane flames containing 0.3% and 1.1% CF_3Br (3, 6-7, 11, 13-14).[4] These studies indicated that the fluorocarbon part of the inhibitor molecule is important to the inhibition process and that reactions of the CF_2 radical are primarily responsible for the formation of the major fluorine-containing species.

---

[1]Research physicist, Pittsburgh Research Center, Bureau of Mines, Pittsburgh, Pa.
[2]Research chemist, Pittsburgh Research Center, Bureau of Mines, Pittsburgh, Pa.
[3]Associate Research Director, AeroChem Research Labs, Princeton, N. J.; formerly research chemist, Bureau of Mines, Washington, D.C.
[4]Underlined numbers in parentheses refer to items in the list of references at the end of this report.

The microstructure of a methane flame containing CF_2Br_2 was chosen for examination to determine the effects of a similar inhibitor molecule. Some questions to be answered by the CF_2Br_2 study include--

1. Does CF_2Br_2 lead to the same or a different set of inhibitor related species in the flame?

2. Is the fluorine chemistry significantly altered by the absence of CF_3?

3. Does the additional Br alter the bromine chemistry?

4. What is the effectiveness of CF_2Br_2 relative to the previously studied CF_3Br?

The CF_2Br_2 microstructure data also provide additional information for clarifying the mechanism of Halon[5] inhibition of methane flames and for obtaining high-temperature reaction rate data.

In this experimental study, the microstructure of a CF_2Br_2-inhibited methane flame is considered. The experimental procedure is briefly discussed, and some background theory is presented to clarify the methods utilized to analyze the data. The results section contains the calculated data (temperature, composition, flux, net reaction rate, and reaction rate coefficient) represented graphically, and observed relationships among the data. In the interpretation section, reasons for the observed relationships are presented. In the conclusion section, the effect of CF_2Br_2 on the flame system is discussed and experimental conditions are considered.

EXPERIMENTAL

The apparatus and techniques used to acquire the flame structure data and the data processing have been previously described (3-7, 9-14, 27-28, 30). A brief description is presented here.

Two premixed flames were examined at 0.042 atmosphere ambient pressure: a slightly lean CH_4-O_2-Ar flame (flame 5) and a similar flame with 1.05 mole-percent CF_2Br_2 added (flame 6). Table 1 contains a summary of the flame characteristics. The flames were stabilized on a water-cooled, porous-plug, flat flame burner with a 10-cm diameter. A stable 1.05% CF_2Br_2-inhibited flame was achieved at a total mass flow rate of 3.2×10^{-3} g cm^{-2} sec^{-1}. The flow rates of methane, oxygen, and argon were controlled by critical flow orifices. A glass flowmeter tube was used for CF_2Br_2 because critical flow orifice conditions could not be attained owing to its low vapor pressure at room temperature. The purity of the CF_2Br_2 was verified by mass spectrometry.

---

[5]Reference to specific trade names is made for identification only and does not imply endorsement by the Bureau of Mines.

TABLE 1. - Characteristics of flames 5 and 6

	Flame 5	Flame 6
Inlet flow rate, g sec^{-1}:		
CH_4	0.0108	0.0108
O_2	0.0455	0.0455
Ar	0.1808	0.1808
CF_2Br_2	0.0	0.0147
Inlet mole-percent:		
CH_4	10.17	10.06
O_2	21.48	21.25
Ar	68.35	67.64
CF_2Br_2	0.0	1.05
v_o[1], cm sec^{-1}	49.07	49.59
T_{max}[2], kelvins	1,853	1,998
T_{ad}[3], kelvins	2,375	[4]2,353
A[5]	1.0 + 0.35z	1.0 + 0.35z
p[6], atmosphere	0.042	0.042

[1]Inlet gas velocity calculated from measured inlet volumetric flow rate and burner surface area.
[2]As measured in the absence of the mass spectrometer sampling probe (5).
[3]Calculated adiabatic flame temperature.
[4]In the absence of measured expermental thermodynamic data for CF_2Br_2, as estimated heat of formation of 99 kcal $mole^{-1}$ was used (38).
[5]Area expansion ratio (dimensionless) expressed as a function of the distance from the burner surface (z) in cm, for $0 < z \lesssim 1$ cm.
[6]Ambient pressure.

Flame gases were sampled directly by a modulated molecular beam mass spectrometer system via a quartz sampling cone. The cone, with an overall outside angle of 39° and an orifice diameter of 87 μm, was designed to minimize flame perturbation and still preserve the identity of radical and intermediate species. A schematic of the system is shown in figure 1.

Composition profiles of stable, intermediate, and radical species were obtained in both flames. The techniques for detecting, identifying, and measuring the observed species were the same as those used in the previous flame studies with the following exceptions. H and O atoms and OH radical concentration profiles were determined from corrected mass spectral intensity measurements and calibration factors that were computed by using the "partial equilibration" concept (12, 31) and the known stable species concentrations in the hot gas region of the flames ($z > 1.0$ cm). The CF_2Br_2 concentration was monitored in the inhibited flame as mass 129 (CF_2Br^+). Calibration of the mass spectrometer system for CF_2Br_2 with the flame 6 inlet gas mixture resulted in erroneously high CF_2Br_2 mole fraction values in the inhibited flame near the burner surface. The reasons for this discrepancy were not determined, and so a calibration factor for the CF_2Br_2 mole fraction profile was selected that forced the initial mole fraction values to equal the known CF_2Br_2 concentration in the inlet gas mixture.

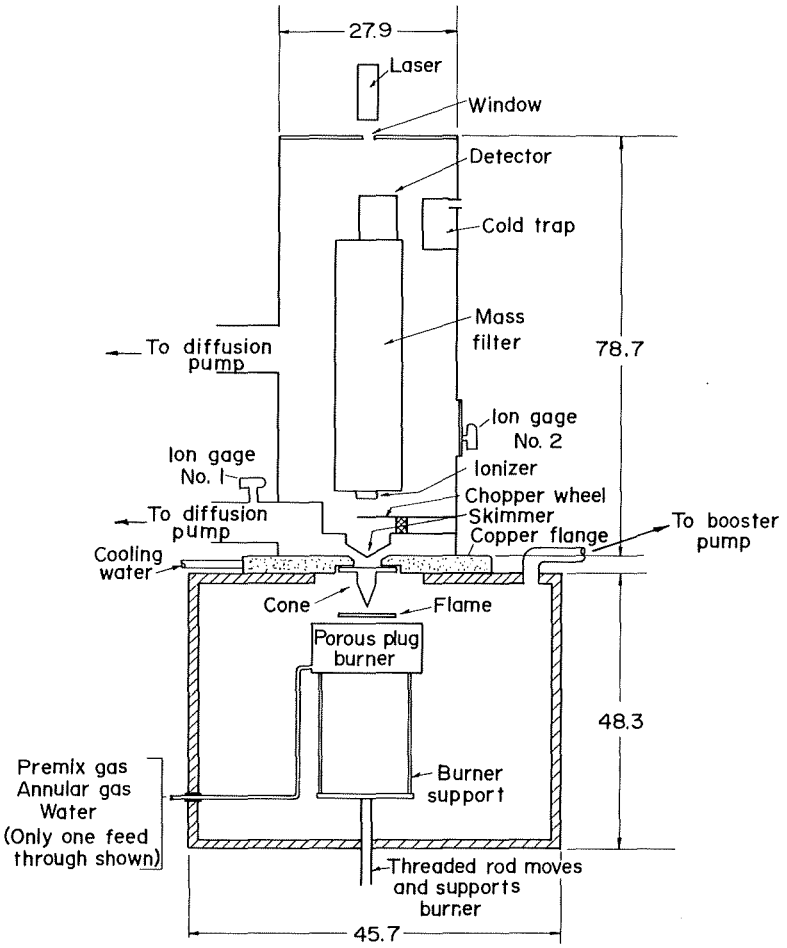

Note: Skimmer orifice to cone tip = 5.8
Skimmer orifice to ionizer = 9.4
Skimmer orifice diameter = 0.25
Cone orifice diameter = 0.0087
All dimensions are centimeters

FIGURE 1. - Molecular beam-mass spectrometer system used to study low-pressure flat flames.

Temperature profiles were determined for each flame with a silica-coated fine wire Pt-Pt 10% Rh thermocouple. The temperatures were corrected for the radiant energy loss of the thermocouple. The area expansion ratio (3) for flames 5 and 6 was assumed to be the same as that experimentally determined for a previous flame of similar initial flow velocity.

The specific details of the experimental apparatus and procedures have been published with respect to the construction and performance of the burner, sampling probe, and mass spectrometer (4); thermocouple construction and temperature measurement (4); probe perturbation of the flame (5); and identification and measurement of stable and radical species (4, 6-7, 9, 12, 27-28).

THEORY

Chemical inhibition results from chemical interference with the normal reaction pathways of a flame. Two fundamental macroscopic characteristics of a flame are adiabatic temperature and adiabatic burning velocity. The burning velocity is a complicated function of several variables, including the collective effect of the chemical reactions and diffusion processes that propagate a flame. A substance is considered a chemical inhibitor when adding a small amount of it to a flame--an amount that does not significantly alter the calculated maximum adiabatic flame temperature--results in a substantial reduction in the adiabatic burning velocity and/or flame extinguishment. The objective of this flame structure study is to identify the mechanisms by which inhibition is achieved. Measured temperatures and species concentrations are translated into species net reaction rates, which are analyzed in terms of elementary chemical reactions and reaction mechanisms.

The method of flame structure analysis is to adopt a physical model by which the measured mole fraction and temperature data are interpreted. This model represents the physical phenomena known to occur in chemically reacting and flowing gas systems. The physical phenomena are convective energy transfer, radiant energy transfer, convective mass transfer, aerodynamic divergence of the gas flow, concentration diffusion, and thermal diffusion. Reference 30 contains a detailed description of the physical model.

Application of an energy balance equation to the thermocouple, considering convective heat transfer from the gas to the thermocouple and radiative heat transfer from the thermocouple to ambient walls, yields an expression for the gas temperature, T_g (24).

$$T_g = T_m + 1.25\ \varepsilon\ \sigma\ d^{3/4}\ (\eta/\rho v)^{1/4}\ (T_m^4 - T_w^4)/\lambda$$

Here, T_m is the measured thermocouple temperature based on the thermocouple voltage and NBS calibration tables (32); ε is the thermocouple emissivity, assumed to be 0.22 (15); σ is the Stefan-Boltzmann constant; d is the thermocouple wire diameter, measured at the Pt-Pt 10% Rh interface; η is the viscosity of the ambient gas; ρv is the ambient gas mass flow rate; T_w is the ambient wall temperature; λ is the ambient gas thermal conductivity.

The value of η and λ are approximated by taking those values for pure argon (21). Since η and λ are dependent upon the unknown gas temperature, the above equation is iterated. First T_g is assumed to be T_m for the purpose of calculating η and λ, then the T_g recalculated using the last calculated value of T_g for the purpose of calculating η and λ until the change in T_g is small.

Through the physical model, species fluxes are calculated from the mole fraction data. Species fluxes are utilized to interpret the dynamics of the flame process. The conservation of atomic species is applied to the data by summing the molecular species fluxes over their atomic constituents. Application of this conservation law provides a measure of the accuracy of the data.

Species net reaction rates, calculated from the species fluxes, are utilized to deduce the chemical mechanism of flame propagation. By comparing these rates between inhibited and uninhibited flames, the chemical mechanism(s) of inhibition may be inferred.

Also, the rate data are used to test the accuracy of the flame structure data. Where a mechanism for the reaction of a species is known and sufficient chemical kinetic data are available, chemical reaction rate coefficients can be calculated from species concentration and net reaction rate data. The consistency of chemical reaction rates determined under similar physical conditions is a measure of the accuracy of the flame structure data.

A quasi-one dimensional model (17, 30) is used to calculate fractional mass flux profiles, G_i, for each species (i) according to the equation

$$G_i = \frac{M_i}{\Sigma_j X_j M_j} \left\{ X_i - \left(\frac{D_{i\text{-}Ar}}{v} \right) \left[\frac{dX_i}{dz} + k_{T_i} \frac{d\ \ln T}{dz} \right] \right\} \qquad (A)$$

where z is the perpendicular distance above the burner surface, X_i is the mole fraction, M_i is the molecular weight, $D_{i\text{-}Ar}$ is the binary concentration diffusion coefficient with argon, k_{T_i} is the binary thermal diffusion ratio with argon, v is the average bulk flow velocity, and T is temperature. G_i represents the fraction of the total mass flux per unit area that is due to species i. Individual species net reaction rates (K_i), the sum of the rates of all reactions forming and all reactions consuming a given species, are calculated as:

$$K_i = \frac{\rho_o v_o}{A(z) M_i} \frac{d}{dz} G_i \qquad (B)$$

where ρ_o and v_o are the cold gas density and velocity, respectively, and A(z) is the area expansion ratio. These net reaction rates, together with the concentrations and temperatures at each position in the flame, are the starting point from which kinetic analyses and deductions about mechanisms are made.

Computing fluxes from mole fractions requires the spatial derivative of the mole fraction profile, and computing of net reaction rates from fluxes requires the spatial derivative of the flux profile. (See equations A and B.) The calculation of derivatives requires a dense set of data points that are relatively smooth. Small variations in the mole fraction profile may result in large oscillations in the net reaction rate profile. To get a smooth, dense set of data, the measured data are interpolated and then smoothed. Smoothing is done by sequentially least-square fitting a second-order polynomial to 25 interpolated data points at a time (30, 34-35). This procedure is repeated until a satisfactorily smooth mole fraction profile is achieved.

The physical models for data analysis, the computation of $D_{i\text{-}Ar}$ and k_{T_i}, some procedures for the reduction of concentration data to net reaction rate profiles (30), and the applicability of these techniques to the determination of chemical reaction rate coefficients have been discussed in detail elsewhere (6, 10).

RESULTS

The thermocouple voltages and mass spectrometric intensities were converted to temperatures and mole fractions. Subsequent analysis yields dimensionless mass fluxes, net reaction rates, and the atomic species conservation profiles. For some reactions, rate coefficients are calculated. These data are graphically presented in this section, and observed relationships among the data are made.

Figure 2 shows unmodified temperature profiles for flames 5 and 6. The solid line represents the uninhibited flame 5, and dashed line represents the 1.05% CF_2Br_2-inhibited flame 6.

For the inhibited flame 6 relative to the uninhibited flame 5, four differences are observed: (i) the maximum flame temperature is greater; (ii) the maximum flame temperature is achieved at a greater distance from the burner surface; (iii) the spacially averaged temperature gradient across the flame zone is smaller; and (iv) the temperature profile inflection point is achieved at a greater distance from the burner surface. Using superscripts "I" and "u" to denote inhibited and uninhibited, respectively, the parentheses to denote functional dependence, and the bar symbol (—) to denote the global or spacially averaged value, these observed relations may be summarized as follows:

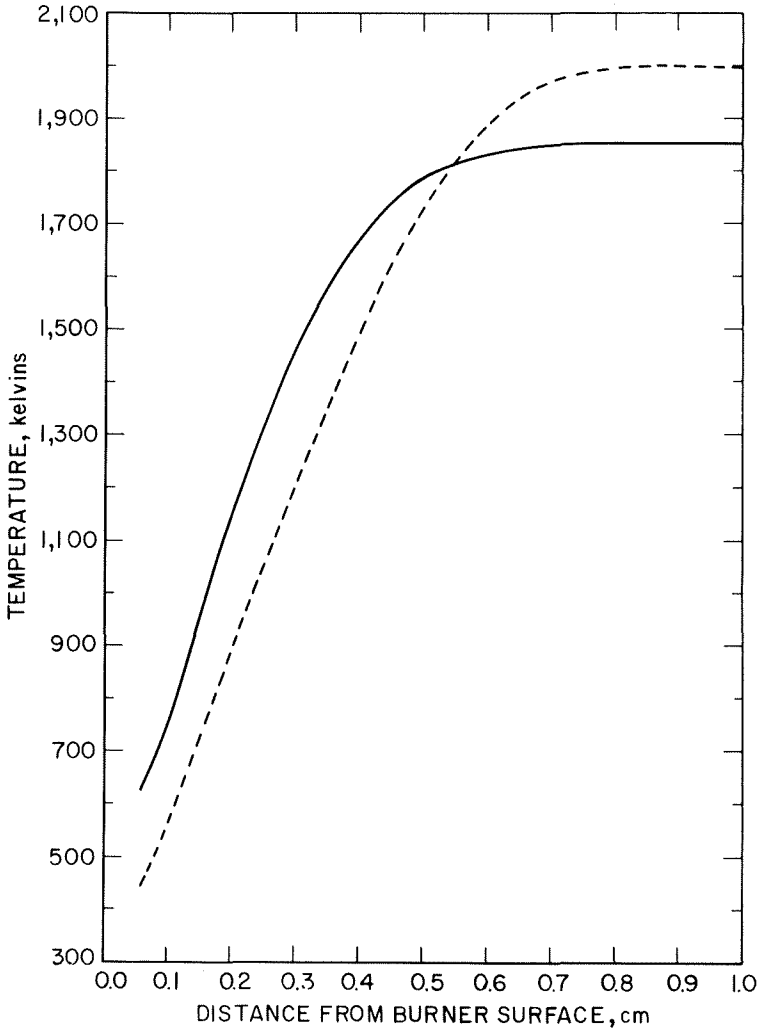

FIGURE 2. - Temperature profiles of the flames studied. The solid line represents the methane-oxygen-argon flame (flame 5). The broken line represents the CF_2Br_2-inhibited flame (flame 6).

$$T_{max}^{I} > T_{max}^{u}$$

$$z\left(T_{max}^{I}\right) > z\left(T_{max}^{u}\right),$$

$$\overline{\frac{dT}{dz}}^{I} < \overline{\frac{dT}{dz}}^{u}$$

$$z\left(\left[\frac{dT}{dz}\right]_{max}^{I}\right) > z\left(\left[\frac{dT}{dz}\right]_{max}^{u}\right)$$

The chemical species identified and measured in the CH_4-O_2-Ar flame (flame 5) are CH_4, O_2, H_2CO, H_2, CO, O, OH, H, CH_3, H_2O, and CO_2. In addition to these chemical species, the following are identified and measured in the CH_4-O_2-Ar flame initially containing 1.05% CF_2Br_2 (flame 6): CF_2Br_2, CH_2CF_2, CH_3Br, F_2CO, HBr, Br, CF_2, Br_2, and HF. Concentration, flux, and net reaction rate profiles are calculated for each of these species.

Figures 3 and 4 show the mole fraction profiles and the temperature profile for flame 5. Figures 5-8 show the mole fraction profiles and the temperature profile for flame 6. In these figures, the symbols

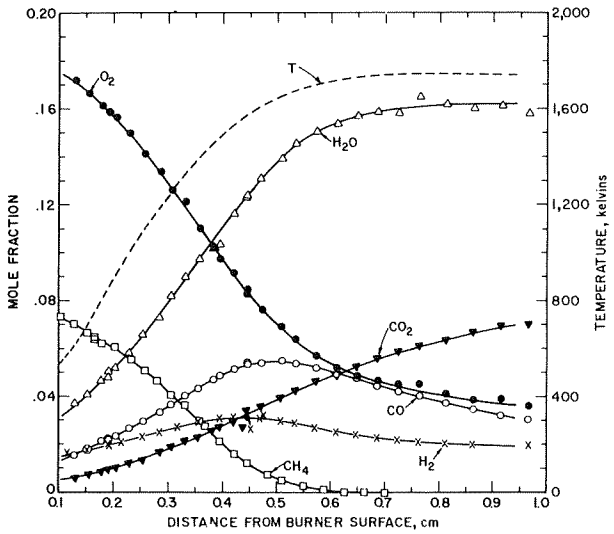

FIGURE 3. - Temperature and composition profiles for the major stable species of the uninhibited flame 5.

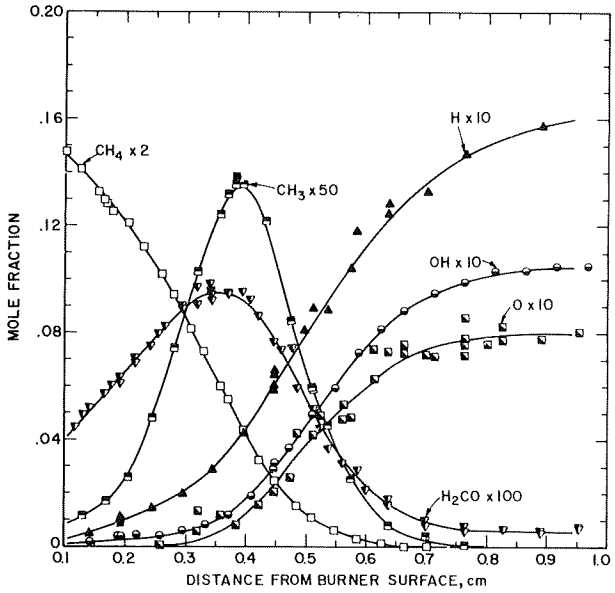

FIGURE 4. - Composition profiles for the intermediate and radical species of the uninhibited flame 5.

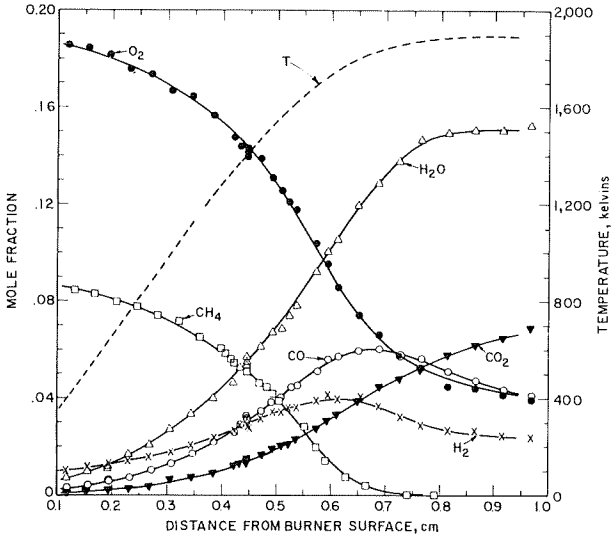

FIGURE 5. - Temperature and composition profiles for the major stable species unrelated to the inhibitor in flame 6.

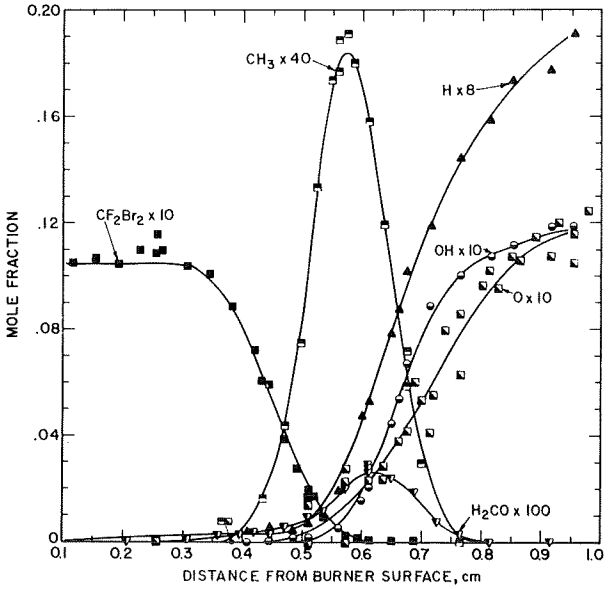

FIGURE 6. - Composition profiles for the principle radical species and the inhibitor in flame 6.

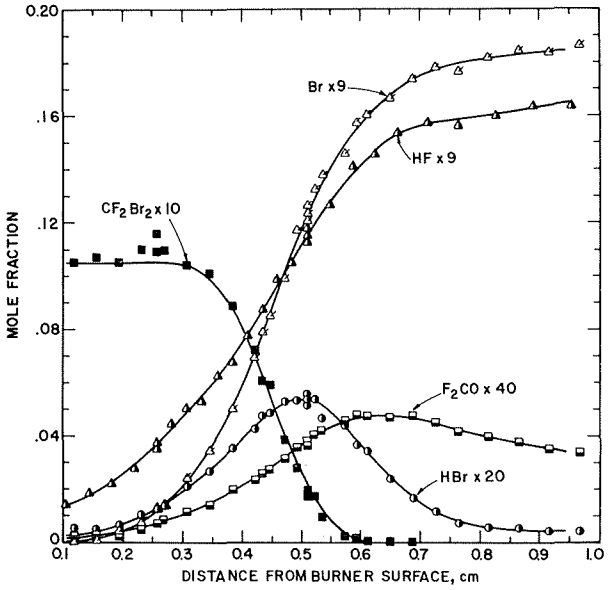

FIGURE 7. - Composition profiles for the major stable and intermediate species related to the inhibitor in flame 6.

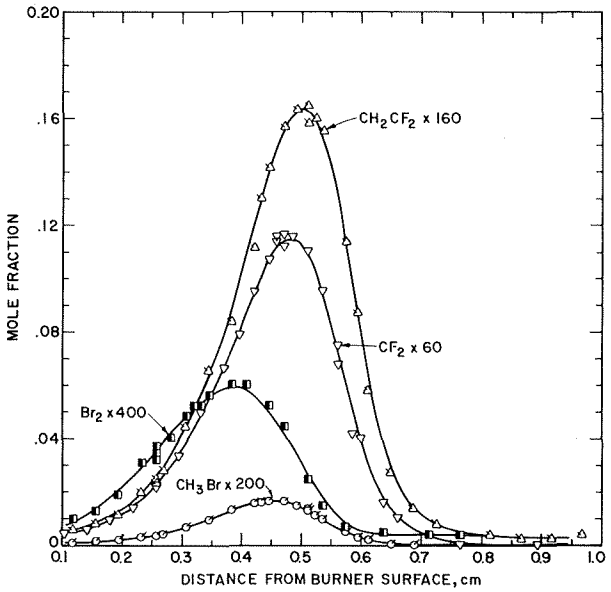

FIGURE 8. - Composition profiles for intermediate species related to the inhibitor in flame 6.

represent data points, the solid lines represent the smoothed mole fraction profiles computed from the data points, and the dashed lines represent the smoothed temperature profiles computed from the temperature data points, which are not represented in these figures. The temperature data are taken in the absence of the mass spectrometer quartz cone sampling probe. The temperature profiles of figures 3 and 5 have been matched to the species profiles by correcting the temperature profiles for the cooling effect of the quartz probe (4-5). Data were taken from the burner surface to a point 13 cm above the burner surface. Since the flame region of interest here is the primary reaction zone, smoothed profiles are calculated only to 1.3 cm and are here represented only to 1.0 cm.

The composition profiles obtained for flames 5 and 6 (figs. 3-8) show for both flames that as the fuel (CH_4) and oxidizer (O_2) disappear, intermediates (H_2CO, H_2, CO) and radicals (O, OH, H, and CH_3) appear. Appearing along with the intermediates and radicals are the stable products (H_2O and CO_2). (Since these flames are slightly fuel lean and equilibrium conditions are not achieved, there is residual O_2.) In addition to these species common to both flames 5 and 6, figures 6-8 show for flame 6 the disappearance of the inhibitor, CF_2Br_2, accompanied by the appearance of the intermediates, CH_2CF_2, CH_3Br, Br_2, F_2CO, and HBr, radicals Br and CF_2, and the stable product HF. Owing to the low ambient pressure (0.042 atm), the secondary reaction zone is greatly extended past 1 cm. This extension makes some of the intermediates and radicals (H_2, CO, H, O, OH, Br, F_2CO) appear as products in these figures at z = 1 cm.

The flame microstructure composition data represented in figures 3-8 reveal five distinguishing features in the comparison of the inhibited flame relative to the uninhibited flame. For the inhibited flame:

i) CH_4 and O_2 disappear initially more slowly, then more rapidly;

ii) H_2, CO, CO_2 and H_2O appear initially more slowly, then more rapidly;

iii) the composition profiles of the species not generated from the inhibitor molecule are shifted to higher temperature;

iv) the maximum concentrations of the species not generated from the inhibitor molecule (except for H, O, OH, CH_3, and H_2CO) are similar;

v) there are many additional (inhibitor generated) species.

Species maximum concentrations are compared in table 2. These show that the concentrations of CO, CO_2, H_2O, OH, and H_2 in flames 5 and 6 are quite similar. H, O, H_2CO, and CH_3 concentrations are quite different.

TABLE 2. - Comparison of flames 5 and 6 species maximum concentrations

Species	Temperature at maximum species concentration, kelvins		Species concentration, mole cm^{-3}		Concentration ratio, flame 6/flame 5
	Flame 5	Flame 6	Flame 5	Flame 6	
CO.....	1,655	1,826	1.70×10^{-8}	1.69×10^{-8}	0.99
CO_2....	1,752	1,895	2.11×10^{-8}	1.86×10^{-8}	.88
H.....	1,752	1,898	4.73×10^{-9}	6.61×10^{-9}	1.40
H_2O....	1,753	1,896	4.76×10^{-8}	4.10×10^{-8}	.86
OH.....	1,753	1,896	3.07×10^{-9}	3.2×10^{-9}	1.04
H_2.....	1,578	1,760	1.01×10^{-8}	1.16×10^{-8}	1.15
O.....	1,753	1,895	2.34×10^{-9}	3.20×10^{-9}	1.37
H_2CO...	1,392	1,778	3.50×10^{-10}	7.57×10^{-11}	.22
CH_3....	1,474	1,697	9.40×10^{-10}	1.39×10^{-9}	1.48

The H, O, and OH radical concentrations are in partial equilibrium where their maximum concentrations are achieved. As a function of temperature the H, O, and OH radical concentrations are reduced in the inhibited relative to uninhibited flame. Figures 9-11 are plots of the mole fraction of H, O, and OH versus temperature for both flames 5 and 6. H, O, and OH concentrations of flame 5 can be compared with those of flame 6. These figures show that at all temperatures common to the inhibited and the uninhibited flame, the H, O, and OH radical concentrations are reduced in the inhibited flame.

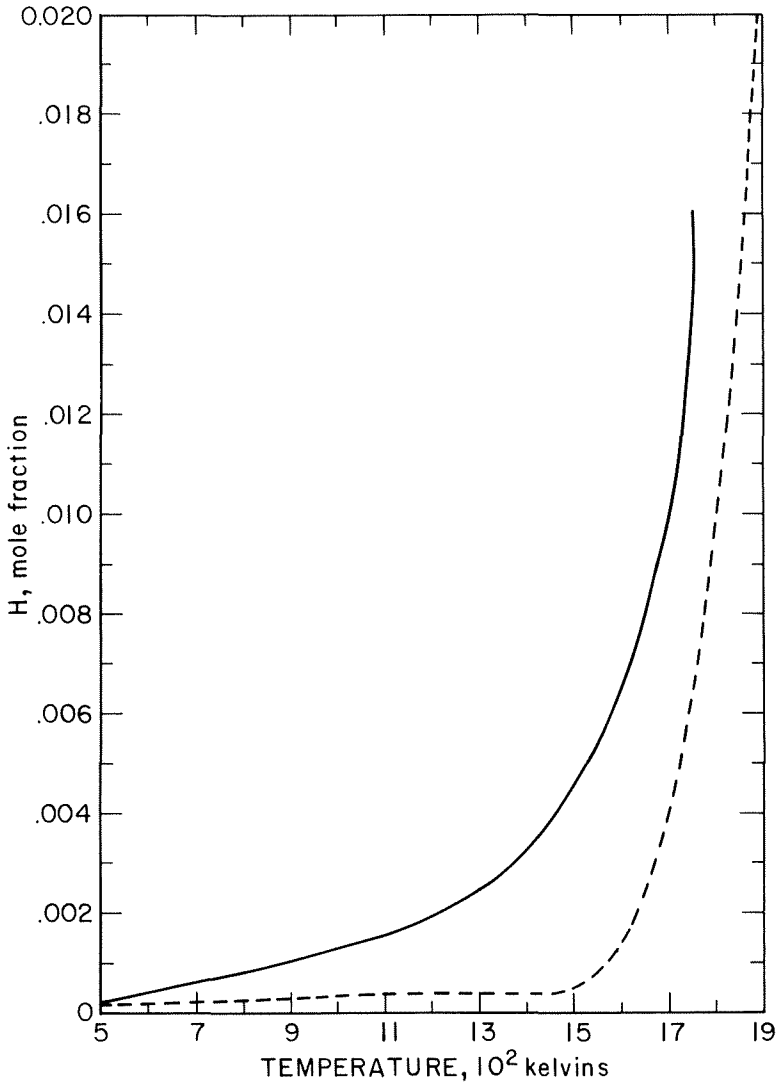

FIGURE 9. - Hydrogen atom mole fraction for flames 5 and 6 plotted as a function of temperature. The solid line represents the uninhibited flame 5. The broken line represents the inhibited flame 6.

Figures 12 and 13--plots of the H_2CO and CH_3 mole fraction versus temperature in flames 5 and 6--allow direct comparison of the H_2CO and CH_3 concentrations. As shown in figure 12, the uninhibited flame H_2CO concentration is greater than that of the inhibited flame. Figure 13 shows that the peak CH_3 concentration in the inhibited flame is greater than that in the uninhibited flame.

Dimensionless mass fluxes were calculated for each species using equation A. Figure 14 gives the salient features of the species flux profiles in the inhibited and uninhibited flames and the direction of the net mass fluxes as a function of temperature. Flame 5 data are represented on the left side of the figure, separated from the flame 6 data on the right side of the figure by the temperature axis at the center. The species symbol is at the temperature of zero flux. An upward arrow indicates positive flux, parallel to the bulk flow. A downward arrow indicates negative flux, anti-parallel to the bulk flow. The fluxes of several species are everywhere positive for $T > 1{,}400$ kelvins. These species are parenthesized at the bottom of the figure. Species fluxes of the inhibited and uninhibited flames are similar in relative order and direction with the inhibited flame zero fluxes all shifted to higher temperature. The figure also shows H, O, and OH radical net fluxes from the high-temperature region to the low-temperature region.

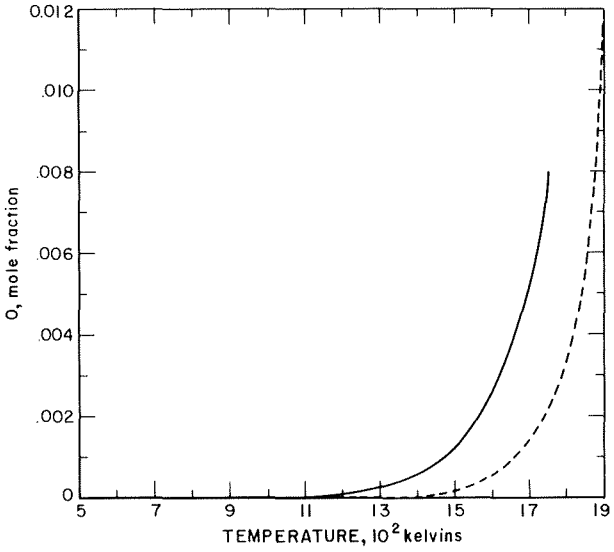

FIGURE 10. - Oxygen atom mole fraction plotted as a function of temperature for the uninhibited (flame 5) and CF_2Br_2-inhibited (flame 6) flames. The solid line represents the uninhibited flame. The broken line represents the inhibited flame.

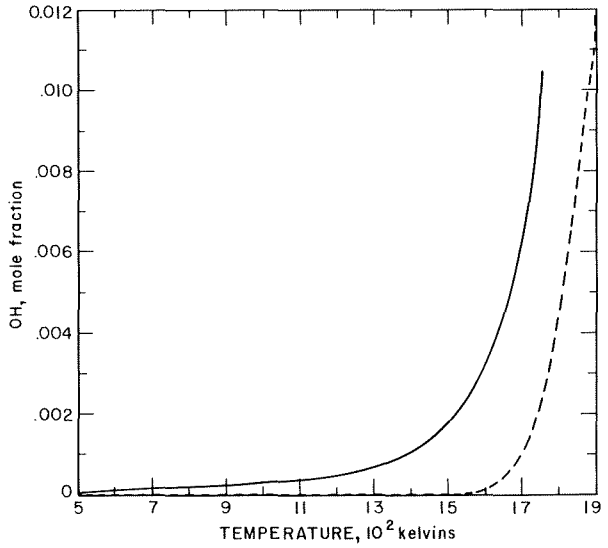

FIGURE 11. - Hydroxyl radical mole fraction versus temperature for uninhibited flame 5 (solid line) and CF_2Br_2-inhibited flame 6 (broken line).

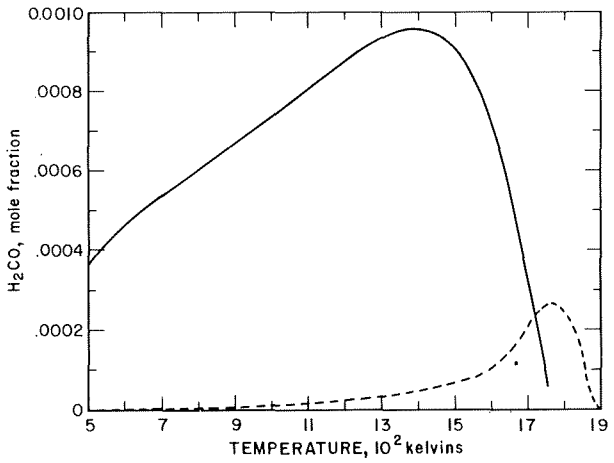

FIGURE 12. - Formaldehyde mole fraction versus temperature. Solid line–uninhibited flame 5. Broken line–CF_2Br_2-inhibited flame 6.

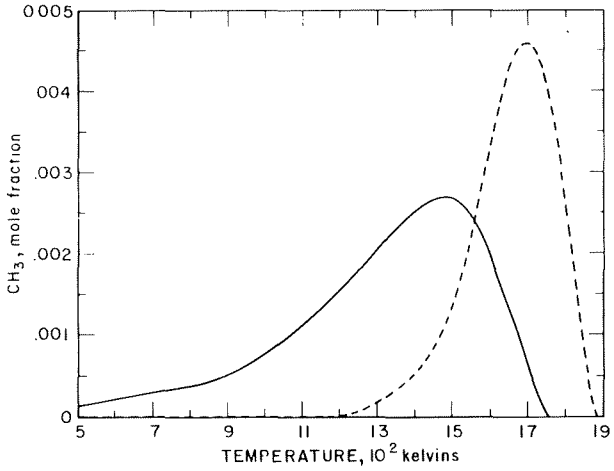

FIGURE 13. - Methyl radical mole fraction versus temperature. Solid line is for flame 5. Broken line is for flame 6.

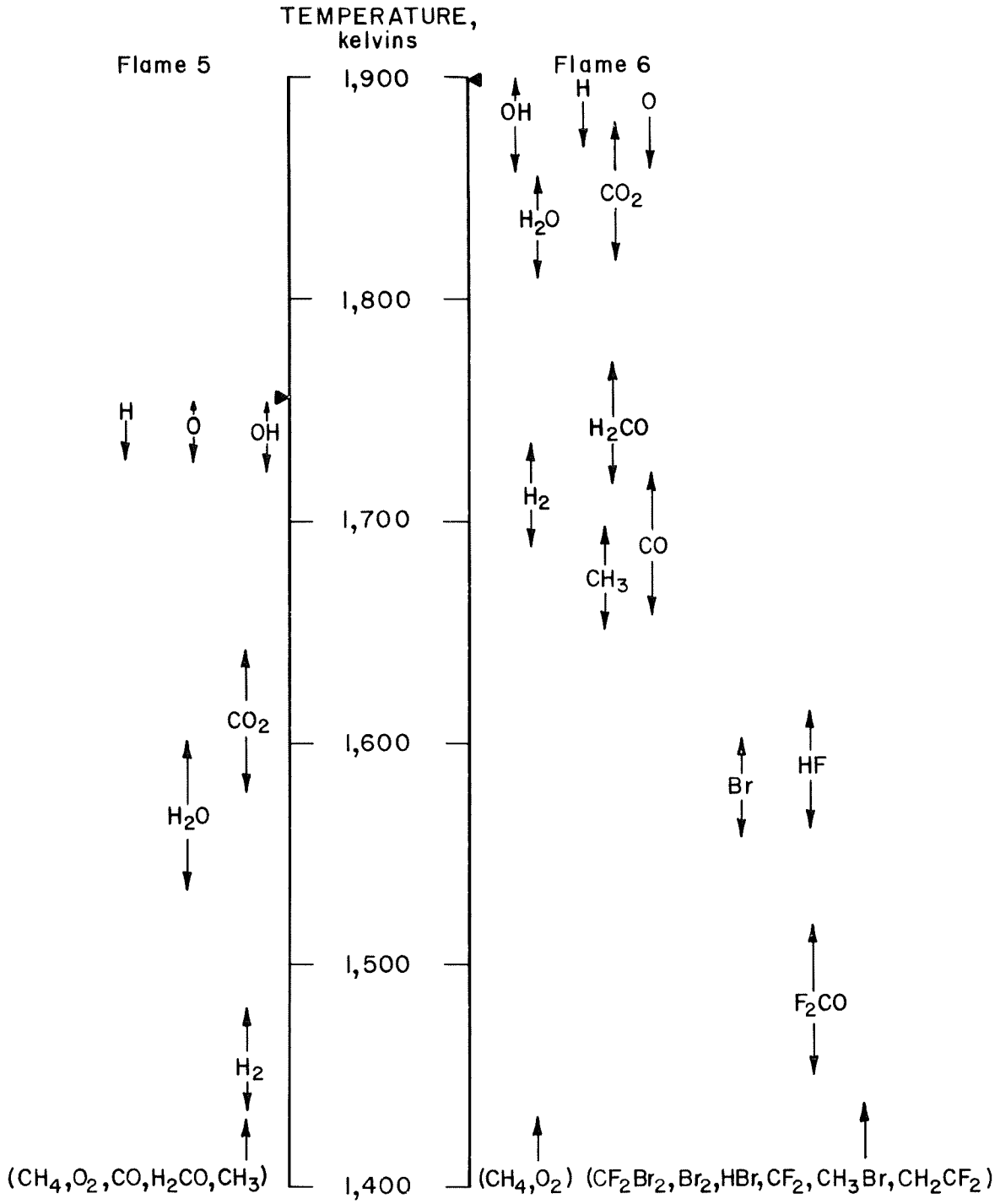

FIGURE 14. - Flux direction versus temperature for flames 5 and 6. Flux directions are represented to the left (flame 5) and right (flame 6) of the central temperature axis. The species labels appear at the temperature where the flux is zero. The solid arrow heads (▶) mark the maximum flame temperatures.

Conservation of atomic species provides a test of the internal consistency and accuracy of the mole fraction data and the computation of the flux profiles from mole fraction profiles. At each point in the flame, the deviation of the net atomic species flux from its known inlet value should be zero. Figure 15 shows the percent deviation from the inlet atomic flux for C, O, and H in flames 5 and 6, and for Br and F in flame 6. These figures show a greater percent deviation from inlet atomic flux for the inhibited relative to the uninhibited flame. The H, F, and Br percent deviation for the inhibited flame are substantial in some regions. The H-atom deviation was considered in terms of the contribution from each hydrogen-containing molecule and of the effect of matching the temperature profile to the species profiles. The flame 6 hydrogen-containing molecular species were also compared with the flame 5 hydrogen-containing molecular species and with the flux profiles of hydrogen-containing species from other inhibited flames. No one species or combination of a few species could be identified as being solely responsible for the significant H-atom deviation from the inlet H-atom flux of flame 6. The inhibited flame hydrogen-containing molecular flux profiles are similar to those of the uninhibited flame and to those of previously studied inhibited flames. No variation of calibration factors or temperature alinement with respect to species profiles could be made that both improved the H-atom conservation in the region of maximum deviation and did not significantly deteriorate the conservation of C, O, F, Br, and/or H in other

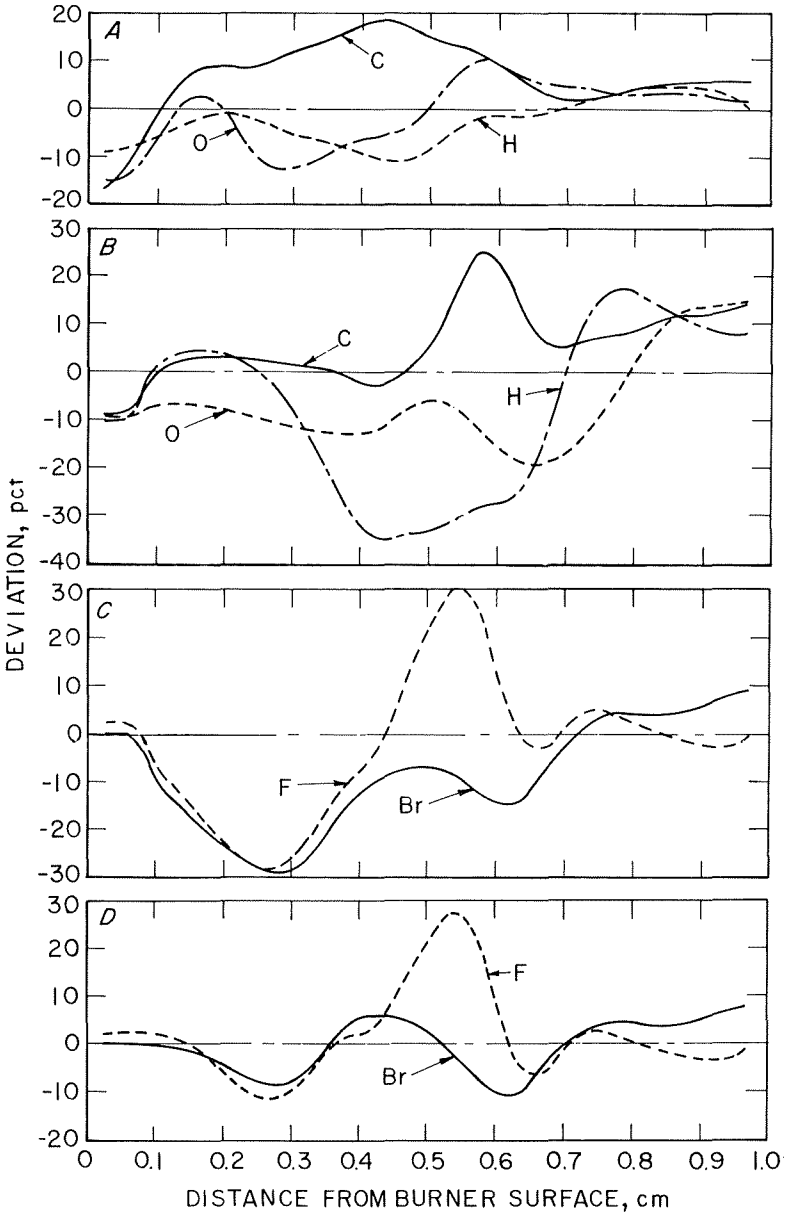

FIGURE 15. - Element conservation based on flux for the uninhibited and inhibited flames. *A*. Carbon, oxygen, and hydrogen in flame 5. *B*. Carbon, oxygen, and hydrogen in flame 6. *C*. Bromine and fluorine in flame 6. *D*. Same as *C* except thermal diffusion is ignored.

regions. At the point of greatest H-atom deviation from inlet H-atom flux the deviation represents a combined effect of the hydrogen-containing molecular fluxes.

F and Br atom conservation deviates substantially from zero at small values of z; this is due primarily to the thermal modeling of the CF_2Br_2 flux. The inclusion of thermal diffusion, however, does not significantly change the value of the CF_2Br_2 net reaction rate at the point of maximum CF_2Br_2 disappearance. Figure 15D is the result of a calculation for flame 6 in which k_{T_i} is set equal to zero for all species.

Net reaction rates have been calculated for each species from the species fluxes according to equation B. Figure 16 summarizes the net reaction rate data. Here, net reaction rate extrema (maximum and minimum values of the net reaction rates) are plotted as a function of temperature for flames 5 and 6. Not shown on this figure is the maximum net reaction rate of Br_2, which occurs at 1,280 kelvins. This figure shows that the relative order of the species net reaction rate extrema are similar for flames 5 and 6. The inhibited flame net reaction rate extrema are shifted to higher temperature and are closer together relative to the uninhibited flame. For both flames, H, O, and OH are produced at high temperatures and consumed at low temperatures. In flame 6, the inhibitor molecule, CF_2Br_2, achieves its maximum rate of disappearance well before the fuel molecule, CH_4. The maximum rate of HBr formation thermally precedes that of HF. HBr disappears at high temperatures, and HF appears as a combustion product.

Figures 17-19 represent some selected net reaction rate profiles; that is, net reaction rate plotted as a function of distance above the burner surface. Abcissa increments are the same, but the ordinate increments of figure 17 differ from those of figures 18 and 19. In these figures, detailed characteristics of major stable species net reaction rates are given for flames 5 and 6.

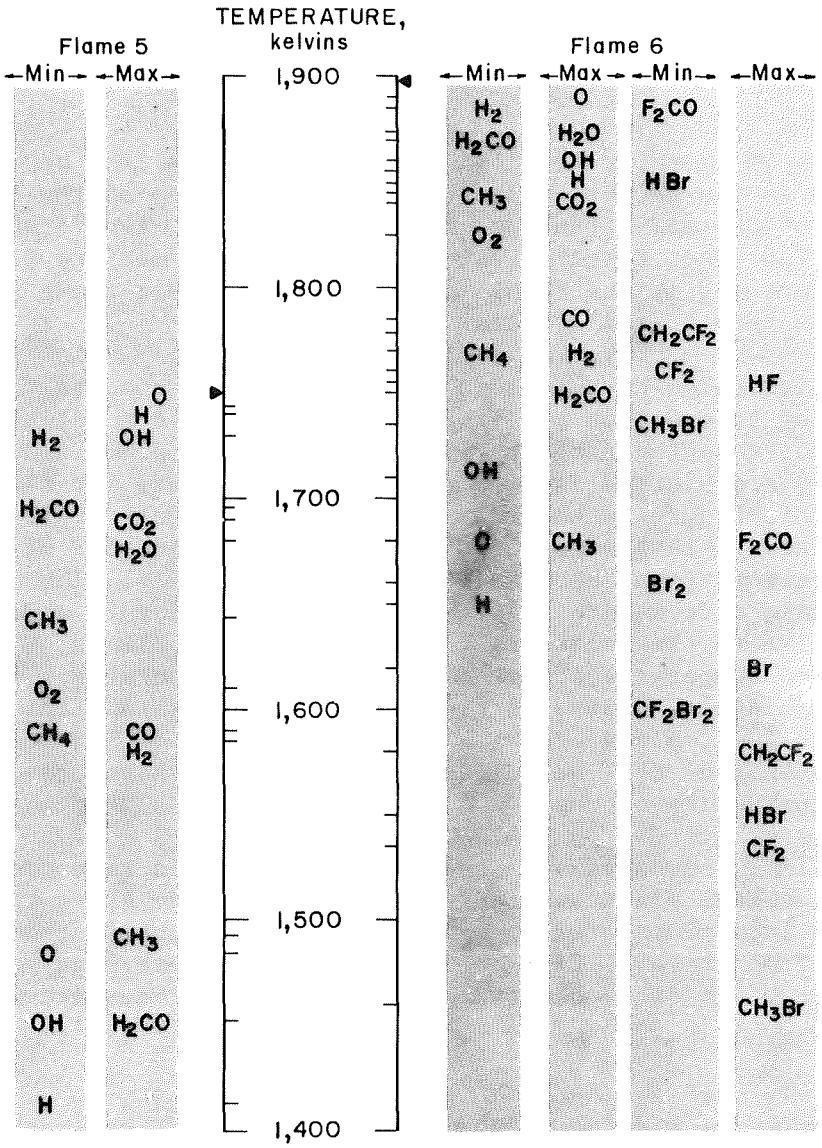

FIGURE 16. - Net reaction rate extrema versus temperature for flames 5 and 6. Minimum (–) and maximum (+) net reaction rates for flame 5 species appear in columns to the left of the central temperature axis. Flame 6 species net reaction rate extrema to the right of the temperature axis are further divided into inhibitor unrelated species to the left and inhibitor related species to the right. The species label appears at the temperature where extremum is achieved. The solid arrow heads (▶) mark the maximum flame temperatures. Missing from this figure is the maximum net reaction rate of Br_2, which occurs at 1,280 kelvins.

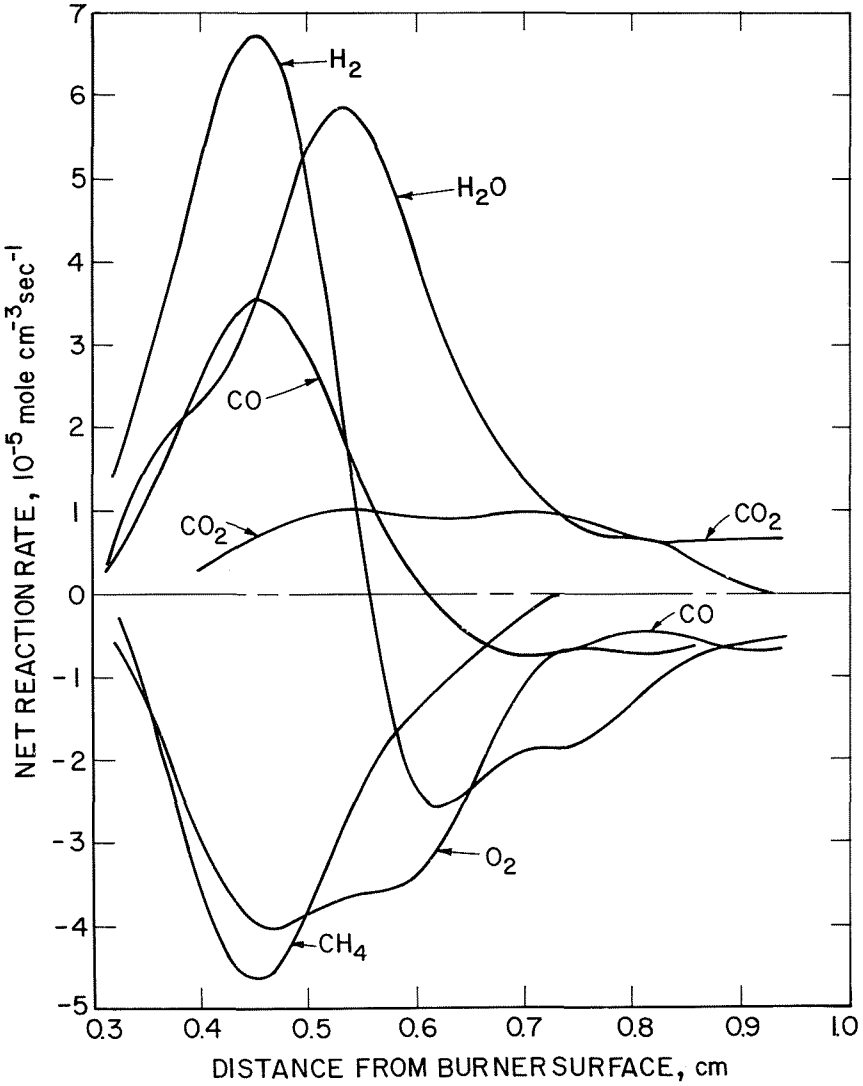

FIGURE 17. - Net reaction rate profiles versus distance above the burner surface for the major stable species of flame 5.

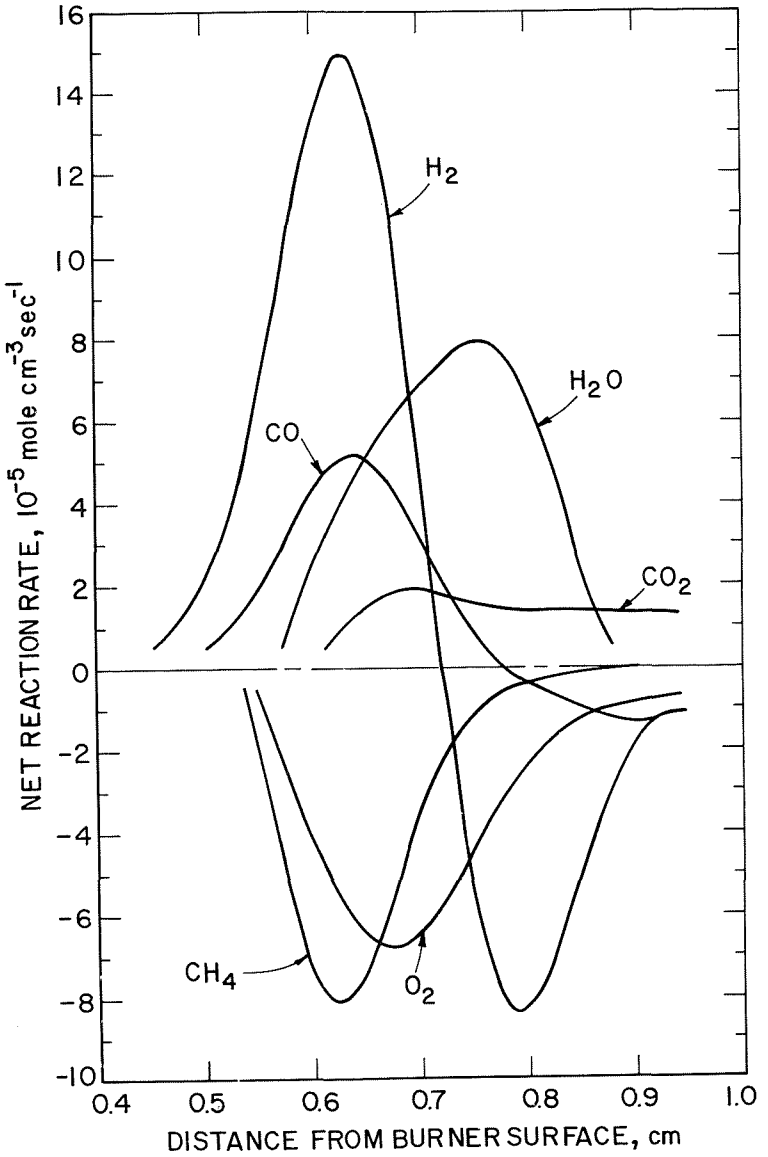

FIGURE 18. - Net reaction rate profiles versus distance above the burner surface for the major stable species of flame 6.

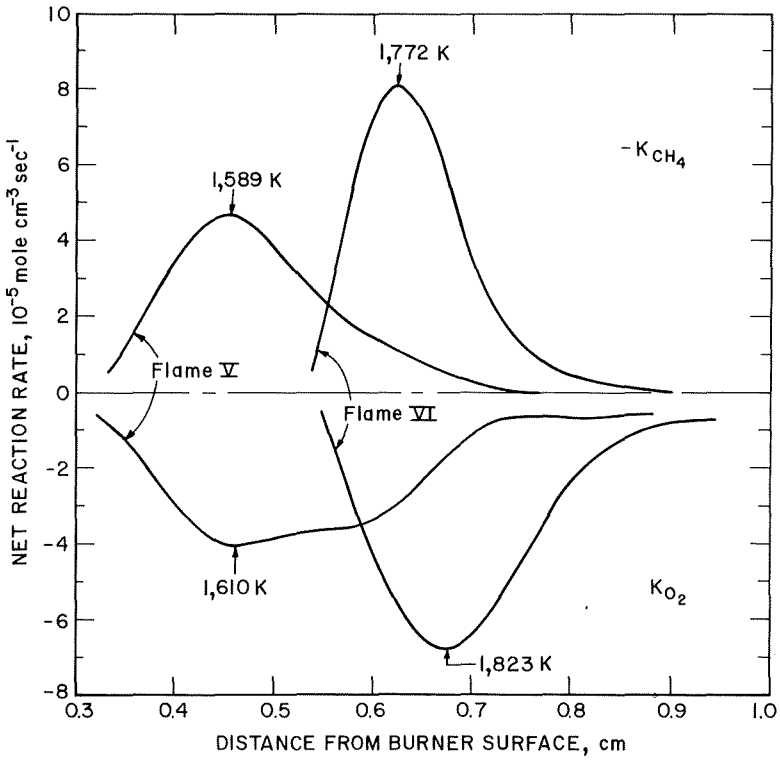

FIGURE 19. - Net reaction rate profiles of CH_4 and O_2 versus distance above the burner surface for flames 5 and 6.

Figures 17 and 18 represent the net reaction rate profiles of CH_4, O_2, CO, CO_2, H_2, and H_2O for flames 5 and 6, respectively. Comparing the two figures shows the extent of net reaction rate shift to higher z values in the inhibited relative to the uninhibited flame. These figures also show that the inhibited flame net reaction rate extrema are greater in magnitude and are closer together. Figure 19 represents the net reaction rate of CH_4 and O_2 for flames 5 and 6 as a function of distance above the burner surface. This figure allows direct comparison of the shift in net reaction rate and the change in amplitude between both flames for CH_4 and O_2; also, the net reaction rate extrema temperatures are given on this figure. Each species common to the inhibited and uninhibited flames shows a shift in net reaction rate to a larger z value and an increase in net reaction rate magnitude at the extrema.

Figure 20 shows the net reaction rate of CF_2Br_2. The broken line is the result of a calculation for which the thermal diffusion ratio was zero. This figure shows that the CF_2Br_2 minimum net reaction rate profile is not significantly affected by setting $k_{T_i} = 0$, despite the dramatic improvement of F and Br species conservation at small values of z (see fig. 15D).

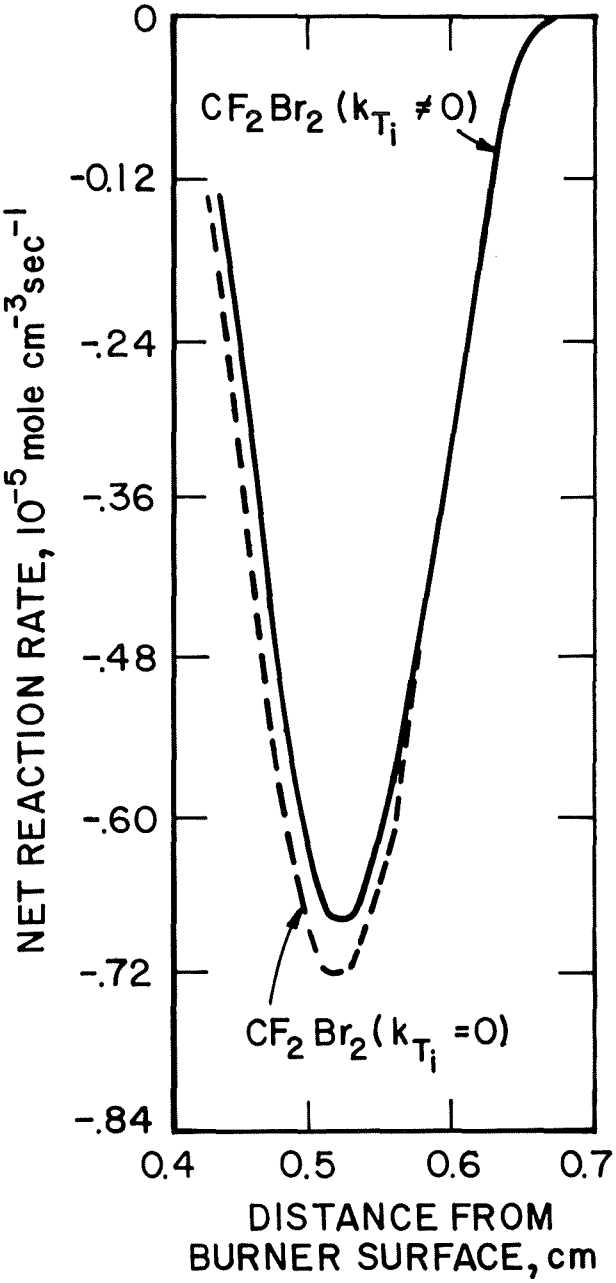

FIGURE 20. - Net reaction rate of CF_2Br_2, with and without thermal diffusion, versus distance above the burner surface. The solid line represents nonzero thermal diffusion ratios. The broken line represents no thermal diffusion.

The chemical reaction rate coefficients for several elementary reactions were calculated in the same manner for both flames 5 and 6. The method and details of these calculations were published in references 6 and 10.

The reactions for which rate coefficients were calculated are:

$$CH_3 + O \rightarrow H_2CO + H, \quad (1)$$

$$H + CH_4 \rightarrow H_2 + CH_3, \quad (2)$$

$$H + O_2 \rightarrow OH + O, \quad (3)$$

and

$$CO + OH \rightarrow CO_2 + H. \quad (4)$$

In figure 21 the rate coefficients for these reactions are plotted versus inverse temperature. The broken lines represent flame 5; the solid lines, flame 6. The flame 5 data cover a temperature range of approximately 1,500 to 1,700 kelvins; flame 6, 1,740 to 1,840 kelvins.

The rate coefficients for reactions 1-4 were also calculated for our previously studied flames. The results represented here are in good agreement with results from those studies (6, 14). Reaction 3 is of particular importance because this reaction has been critically evaluated (1). This coefficient agrees well with that recommended in reference 1.

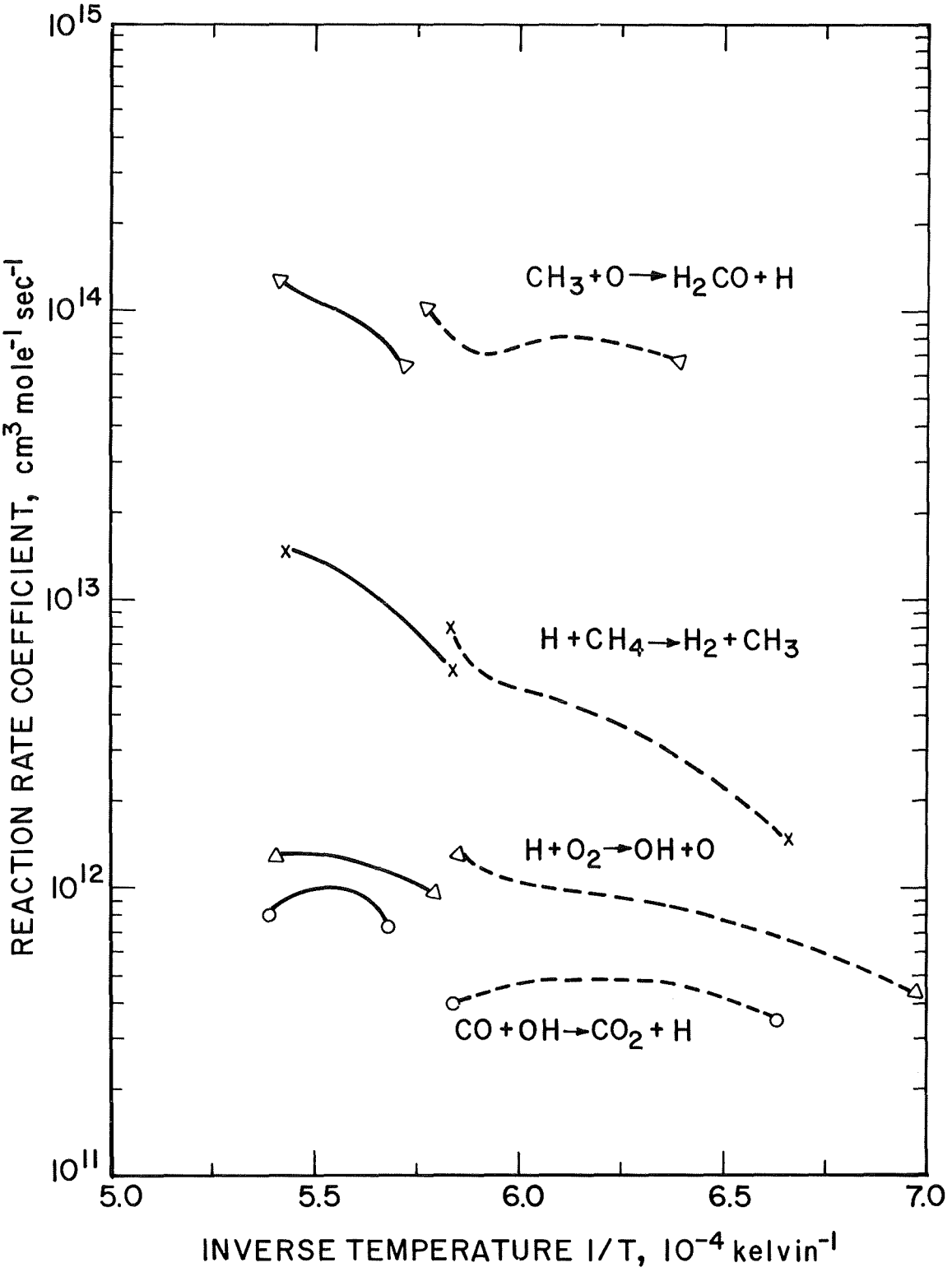

FIGURE 21. - Chemical reaction rate coefficients versus inverse temperature for several elementary reactions occurring in methane flames. The solid lines represent the CF_2Br_2-inhibited flame 6. The broken lines represent uninhibited flame 5.

INTERPRETATION

The reasons for the observed relationships among the calculated data shall now be considered. Of the many differences noted between the clean and the 1.05% CF_2Br_2-inhibited flame, consider first the temperature profile differences, then the composition profile differences.

Temperature

The overall temperature characteristics are explicable in terms of the overall heat-transfer characteristics of the burner-gas system and the effect of inhibitors on burning velocity.

The overall temperature characteristics of the inhibited flame result from the complex interaction between chemical-physical effects of the inhibitor and the physical process of flame stabilization. To relate these processes, consider these two characteristic velocities: v_a, the adiabatic burning velocity, and v_p, a nonadiabatic burning velocity. The adiabatic burning velocity is a property of the gas mixture, the ambient pressure, and the initial temperature. It is the maximum attainable flame propagation velocity and is achieved when the gases react adiabatically.

The flame propagation velocity or the nonadiabatic burning velocity is a variable quantity having the adiabatic burning velocity as an upper bound. The exact value of the flame propagation velocity is dependent upon how much heat is lost from the flame system. Heat loss is dependent upon experimental conditions. Inhibitor-induced flame propagation velocity reduction measurements under identical experimental conditions are a traditional method of determining inhibitor effectiveness. Generally, under adiabatic conditions, the presence of an inhibitor reduces the burning velocity; that is, $v_a{}^u - v_a{}^I > 0$. However, on a cooled flat flame burner, flame stabilization is achieved when sufficient heat is abstracted from flame gases to reduce v_a to v_p. Also, for a stable flat flame, v_p equals v_o, the inlet gas flow velocity. Let Δv be the reduction in velocity due to heat loss to the burner. For the uninhibited flame, $v_p{}^u = v_a{}^u - \Delta v^u$, and for the inhibited flame, $v_p{}^I = v_a{}^I - \Delta v^I$. Since $v_o = v_p{}^u \simeq v_p{}^I$ (see table 1), $v_a{}^u - \Delta v^u = v_a{}^I - \Delta v^I$. But $v_a{}^u - v_a{}^I > 0$, therefore $v_a{}^u - v_a{}^I = \Delta v^u - \Delta v^I > 0$. Thus, heat loss from the uninhibited flame is greater than heat loss from the inhibited flame. This reduced heat loss results in the higher maximum flame temperature of the inhibited relative to the uninhibited flame, $T^I_{max} > T^u_{max}$.

Two other factors that may contribute to the temperature variation between flames are (i) the variation of heat capacity and (ii) the added energy carried into the flame by CF_2Br_2. Since CF_2Br_2 is added to the uninhibited flame mixture (instead of displacing part of the mixture), the heat capacity of the mixture probably increases simply because there are more atoms (molecules) present to absorb heat. However, a gas composition redistribution from high to low heat capacity compounds may occur. A thermodynamic equilibrium computer calculation (18) of the adiabatic flame temperature yields a lower temperature for the CF_2Br_2-inhibited flame. This result implies that the combined effect of added enthalpy and changed heat capacity alone would yield a lower adiabatic maximum flame temperature for the inhibited flame.

The reduced overall temperature gradient in the inhibited relative to the uninhibited flame is a result of the reduced heat loss of the inhibited flame. Energy is transferred from the flame gas system to the burner by thermal conduction and by radical recombination at the burner surface. For thermal conduction,

$$\Delta E_\lambda = \overline{\lambda(\Delta T/\Delta z)},$$

where the units of ΔE_λ are calories cm^{-2} sec^{-1}. Here λ is the thermal conductivity of argon and $\overline{\Delta T/\Delta z}$ is $(T_{max}-T_o)/z(T_{max})$. For radical recombination at the burner surface, the energy transferred to the burner is the sum of the products of the radical fluxes to the burner with the radical heats of formation less the sum of products of the flux of the recombination products with the recombination products heats of formation. For both the inhibited and uninhibited flames, the only radicals with significant fluxes both near and toward the burner surface are hydrogen atoms and hydroxyl radicals. The flux and heat of formation of hydrogen atoms are each 10 times that of hydroxyl radicals. This means that hydrogen atom recombination at the burner surface transfers 100 times more energy to the burner than the next greatest contributor. Considering only hydrogen atom recombination and assuming all hydrogen atoms recombine to form H_2, calculation shows that the amount of energy transferred by radical recombination is less that 4% of the energy transferred by thermal conduction. So energy transfer by radical recombination can be ignored and only energy transfer by thermal conduction considered.

It has been shown above that $\Delta E^I < \Delta E^u$. Applying this condition once again to the overall energy transfer yields,

$$\overline{\left(\frac{\Delta T}{\Delta z}\right)}^I < \overline{\left(\frac{\Delta T}{\Delta z}\right)}^u.$$

The second observed overall temperature difference follows from the two explained above. With a higher maximum temperature and smaller overall temperature gradient, the position (distance from the burner surface) of the maximum temperature must be greater in the inhibited flame.

The effect of a chemical inhibitor is to reduce the adiabatic burning velocity of the flame and, depending on the amount of inhibitor added, to reduce the adiabatic flame temperature. Methane is a self-inhibiting fuel (25). As the equivalence ratio, ϕ, is changed from ϕ=1, the burning velocity is reduced (25, 39) and, for a premixed quenched flat flame, the maximum flame temperature is increased (25, 33). Standoff distance on a flat flame burner, as measured by the inflection point of the temperature profile, has been shown to depend on maximum temperature and propagation burning velocity (16). The standoff distance is a minimum at ϕ=1. To the extent that the addition of inhibitor is equivalent to self-inhibition in its effect upon adiabatic burning velocity, the movement of the inflection point of the temperature profile away from the burner surface upon addition of inhibitor is consistent with the experimental observation of Ferguson and Keck (16).

The phenomena of temperature rise resulting from the addition of inhibitor at constant (flame propagation) velocity has been suggested as a measure of inhibition (22). Results using this technique as a measure of inhibition for gaseous inhibitors at low pressure have been reported for CF_3Br (8) and CH_3Br (19). The technique has been refined (19) and compared with other measures of inhibition (33). Utilizing this method to determine the effectiveness of CF_2Br_2, as was done with CF_3Br in reference 8, it was found that 1% CF_2Br_2 is no more effective than 1% of CF_3Br.

Composition

Interpretation of flame 5 and 6 composition data is based on the chemical reaction rate coefficients of elementary reactions where that is possible. For those species not susceptible to such interpretation, inferences will be drawn from the species net reaction rate extrema or composition profiles. The disappearance of CH_4 and O_2 will be interpreted in terms of their elementary reactions and local radical concentrations. The maximum concentrations achieved by CH_3 and H_2CO will be interpreted in terms of elementary reactions, reaction rate coefficient temperature dependence, and local radical concentrations. The net reaction rate of CF_2Br_2 will be interpreted and a reaction rate coefficient inferred. The reduced radical (H, O, OH) concentrations will be explained considering net reaction rate extrema and the addition of inhibitor-related species. All of the inhibitor-related species observed in this CF_2Br_2-inhibited flame were previously observed in CF_3Br-inhibited flames (6, 14). Also, the observed changes noted in the results section upon addition of CF_2Br_2 are similar to changes previously observed upon addition of CF_3Br.

The primary mechanism of methane disappearance in nearly stoichiometric or slightly lean methane flames is reaction 2. The calculated chemical reaction rate coefficient for this reaction is shown in figure 21 for flames 5 and 6. The rate coefficient was calculated in the same way for both flames. Continuity of the rate coefficient from the flame 5 to the flame 6 temperature domain implies the same mechanism for CH_4 disappearance in both flames 5 and 6. The CH_4 minimum net reaction rate shift to higher temperature in the inhibited relative to the uninhibited flame (figs. 16 and 19) is the result of reduced radical concentrations in the inhibited flame (figs. 9-11).

The same argument can be applied to O_2 disappearance based on reaction 3. Since all other species common to the inhibited and uninhibited flame result from the decomposition of CH_4 and O_2, they too would have net reaction rate extrema shifted to higher temperature (figs. 16-18). Since rate coefficients usually increase with temperature, the same reaction occurring at higher temperature would proceed more rapidly. Thus, narrower and larger magnitude net reaction rates (figs. 17-19) and the greater composition profile gradients are observed (figs. 3-8) in the inhibited relative to the uninhibited flame.

The chemical reaction rate coefficients calculated for reactions 3 and 4 can be compared to evaluated rate coefficients and to rate coefficients calculated from other flame data. The recommended rate coefficient for reaction 3 is $k = 2.2 \times 10^{14} \exp(-8450/T)$ $cm^3\ mol^{-1}\ sec^{-1}$ (1), and for reaction 4 is $\log k = 10.83 + 3.94 \times 10^{-4}\ T$; the units of k are $cm^3\ mol^{-1}\ sec^{-1}$ (2). The

rate coefficient data from flame 5 lies within the recommended error bounds (±30%) and slightly below the recommended value for reaction 3 ($H + O_2 \rightarrow OH + O$) and mostly within the recommended error bounds (±50%) and above the recommended value for reaction 4 ($CO + OH \rightarrow CO_2 + H$). The rate coefficient from the flame 6 data is low for reaction 3 and high for reaction 4 relative to the recommended values. The rate coefficients calculated from flame 5 data lie within the values calculated from previously studied flames. The rate coefficient calculated from flame 6 data are low for reaction 3 and high for reaction 4 relative to those from previously studied flames.

In flame 6, the reaction rate of CH_4 with Br is significant at low temperatures ($T < 1{,}270$ kelvins). Calculation of the net reaction rate of CH_4 was based on experimentally measured temperature and concentrations of CH_4, H, O, OH, and Br. The following reactions were considered:

$$CH_4 + H \rightarrow CH_3 + H_2, \tag{2}$$

$$CH_4 + Br \rightarrow CH_3 + HBr, \tag{5}$$

$$CH_4 + OH \rightarrow CH_3 + H_2O, \tag{6}$$

and

$$CH_4 + O \rightarrow CH_3 + OH. \tag{7}$$

The rate coefficients used for reactions 5, 6, and 7 may be found in references 26, 31, and 20, respectively. The rate coefficient used for reaction 2 extrapolated from the uninhibited flame data. Calculations based on the above set of reactions and the measured CH_4 net reaction rate in flame 6 show that the disappearance of CH_4 is initially dominated by reaction 5 up to 1,250 kelvins and subsequently dominated by reaction 2. Even in flame 6, of all the CH_4 which is consumed, most of it is consumed by reaction 2.

Unlike the H, O, and OH radicals, the maximum CH_3 radical concentration increases in the inhibited relative to the uninhibited flame (fig. 13, table 2). The primary mechanism for methyl radical production is reaction 2. Methyl radical disappearance is associated with the appearance of H_2CO by reaction 1. There is less H_2CO in the inhibited flame (fig. 12, table 2).

The increased maximum CH_3 concentration in the inhibited flame is the result of a greater formation rate due to the shift of the primary reaction zone to higher temperatures. Reaction 2 is the primary path for CH_3 production, and reaction 1 the primary path for CH_3 consumption. The rate coefficient for reaction 2 increases with temperature, while that of reaction 1 does not substantially change with temperature (fig. 21). At the point of maximum CH_3 formation in the inhibited compared with that in the uninhibited flame, $[H][CH_4]$ is slightly smaller and $[CH_3][O]$ is larger. Thus, the increased maximum CH_3 concentration observed in the inhibited flame results from the greater temperature dependence of the rate coefficient of reaction 2 relative to reaction 1.

The decreased maximum H_2CO concentration in the inhibited flame results from an increased consumption rate. Reaction 1 is the primary reaction forming H_2CO. The rate coefficient of reaction 1 does not increase substantially with temperature. At the maximum H_2CO formation rate in the inhibited relative to the uninhibited flame, $[CH_3][O]$ is greater. Thus the reduction of the H_2CO concentration in the inhibited flame must be a result of the increased H_2CO consumption by subsequent abstraction reactions with H, O, and OH and thermal decomposition (31).

The inhibitor, CF_2Br_2, achieves its maximum disappearance rate well before the CH_4 (fig. 16). The inhibitor molecule decomposition is due primarily to thermal decay and H-atom abstraction reactions. The thermal decay of CF_2Br_2 can be of two modes (29, 36):

$$CF_2Br_2 \rightarrow CF_2Br + Br, \tag{8}$$

$$CF_2Br_2 \rightarrow CF_2 + Br_2. \tag{9}$$

The rate coefficients of reactions 8 and 9 have not been determined. The CF_2Br_2 maximum disappearance rate (fig. 20) is 6.7×10^{-6} mole cm^{-3} sec^{-1} at 1,600 kelvins.

The CF_2Br_2 thermal decay coefficient was calculated from the CF_2Br_2 net reaction rate, assuming that thermal decay and hydrogen abstraction reactions predominate in the disappearance. For this analysis, the rate coefficient for the CF_2Br_2 abstraction reaction with H was assumed to be the same as, or twice that, previously determined for CF_3Br (7). The first-order thermal decomposition rate coefficient for CF_2Br_2 is $5.8\ (\pm 2.5) \times 10^3$ sec^{-1} at 1,600 kelvins. This corresponds to 24% to 62% of the CF_2Br_2 consumption rate being due to thermal decomposition. Figure 22 shows the thermal decomposition rate coefficient of CF_2Br_2 plotted as a function of inverse temperature.

The radical population of H, O, and OH as a function of temperature is found to be significantly reduced in the CF_2Br_2-inhibited flame (figs. 9-11). Of the possible causes for this effect--that is, (i) movement of the flame relative to the burner surface, (ii) simple physical effect of the inhibitor (thermal effects), and (iii) chemical interference with the radical chain propagating and branching reactions--only chemical interference is responsible.

Movement of the flame away from the burner surface is a result of the reduced adiabatic burning velocity of the inhibited flame. Movement of the flame relative to the burner surface may also be achieved by varying the inlet gas bulk flow velocity, and this was done for an uninhibited flame. The H, O, and OH species profiles for two flames of the same stoichiometry (10% CH_4, 21% O_2, 69% Ar) and different initial bulk flow velocity (79 cm sec^{-1}, 48 cm sec^{-1}) were compared as a function of temperature. There is a slight change of radical concentration at lower temperature as a result of inlet gas bulk flow velocity change. This reduction is small compared with that observed when the inhibitor is added. For all uninhibited flames, the shapes of the radical profiles are similar, and this shape differs from that of the

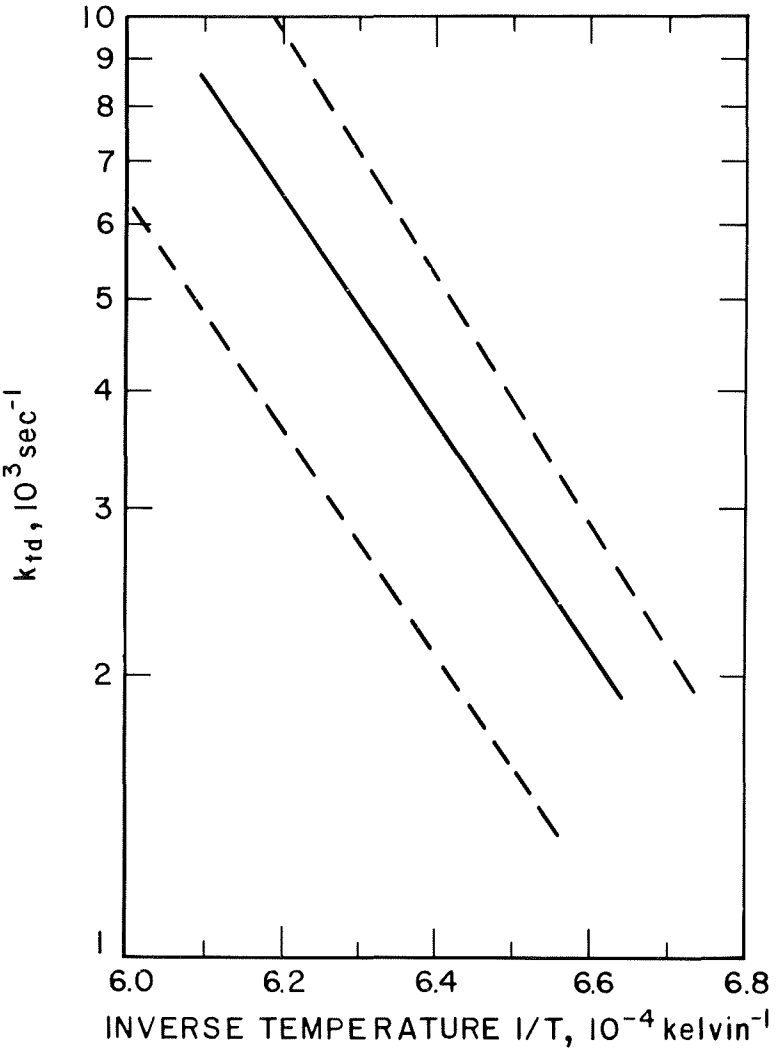

FIGURE 22. - Thermal decomposition rate coefficient for CF_2Br_2 versus inverse temperature. The broken lines represent a calculated coefficient assuming the $CF_2Br_2 + H$ reaction rate coefficient to be equal to (upper), and twice that (lower), of $CF_3Br + H$. The solid line represents an average of the broken line values.

inhibited flame radical profiles. The ininhibited flame radical profile as a function of temperature is concave upward and appears to have two nearly linear regions, one of small slope at low temperature and one of large slope at high temperature, connected by a sharply curved segment. These quantitative and qualitative differences among radical profiles from flames of varying flame propagation velocity, due to inhibitor addition and inlet bulk flow velocity variations, implies that the variation of radical profiles observed in the inhibited relative to the uninhibited flame is not a result of flame movement with respect to the burner surface.

The maximum rate of formation of HBr (~1,550 kelvins) and HF (~1,755 kelvins) occurs before the maximum rate of disappearance of CH_4 (~1,770 kelvins). Both HF and HBr reduce the H-atom population available for reaction with CH_4. The HF concentration is much greater than the HBr concentration (fig. 7) throughout the flame. The HF half maximum rates of formation are at 0.5 and 0.7 cm, and those of HBr are at 0.425 and 0.575 cm. The high concentration of HF below the region of maximum formation rate is due to back diffusion. At higher temperature, the HBr disappears, possibly supplying H-atoms for diffusion into the primary reaction zone. HF is a product, removing H-atoms from the system. HBr and HF both remove H-atoms; HBr acts first, followed by the greater H-atom removal by HF.

The complex physical chemical mechanism by which CF_2Br_2 inhibits the methane flame may be inferred from the net reaction rate data shown in figure 16. CF_2Br_2 disappears before the CH_4. Br_2, CH_3Br, CF_2, HBr, CH_2CF_2, Br, F_2CO, HF, and CH_3 are all formed at their maximum rate before CH_4 reaches its

maximum rate of disappearance. This would imply that the inhibitor and its reaction products are removing H, O, and OH, chain carriers that would otherwise react with CH_4 and O_2.

CONCLUSIONS

The effects of CF_2Br_2 on the temperature and composition profiles of a methane-oxygen-argon flame have been experimentally studied. The inhibited flame temperature characteristics have been explained in terms of the inhibitor effect on the adiabatic burning velocity. Utilizing a computerized physical model of the flame system, species fluxes and net reaction rates have been calculated. The effect of CF_2Br_2 on species profiles has been explained in terms of elementary chemical reactions, where possible. Other interpretations have been made based on calculated net reaction rates.

The H, O, and OH species exhibit several similar characteristics between the inhibited and uninhibited flames in that for both flames they are produced at high temperatures (fig. 16), diffuse to the lower temperature region of the flame (fig. 14), and are consumed in the low-temperature region of the flame (fig. 16). These species characteristics are substantially different in that their net reaction rate extrema are greater in magnitude and delayed to higher temperature, and their concentrations are everywhere reduced at temperatures common to both flames. Of these three species, H reduction is greatest. This reduction in chain-propagating radical concentration, especially H, may cause a shift of flame propagating reactions to higher temperatures, which in turn results in concentration profile shifts to higher temperature.

HF and HBr are seen to appear at relatively low temperatures. Both reduce the number of H-atoms available to participate in the flame reaction pathways. HF is a stable product and does not decompose at higher temperatures. The HBr is not stable. It is an intermediate that disappears at higher temperature, so it may add to the high-temperature formation of atomic hydrogen, which diffuses into the primary reaction region.

The concept of a region of inhibition preceding the primary reaction zone (37) is supported by this study. Numerous inhibitor-related species are identified that have maximum rates of formation preceding the methane maximum rate of disappearance. In addition, the CF_2Br_2 itself reaches a maximum rate of decay before the methane.

The data presented here do not directly support the concept of inhibitor effect due to reduced radical concentrations past the primary reaction zone (23). The larger radical populations observed in the burned gas zone of flame 6 are a result of partial equilibrium amongst the radicals H, O, and OH at the higher maximum temperature achieved in flame 6 relative to flame 5 (see table 2). The higher temperature has been identified as being due to a reduction of heat loss to the burner required for flame stabilization; that is, a result of the experimental technique utilized. That the radicals (H, O, OH) diffuse from the high- to low-temperature regions is demonstrated by the fluxes. So any reduction of radical population at high temperatures would reduce the concentration gradient down which these radicals diffuse and,

therefore, reduce the radical (H, O, OH) fluxes to the primary reaction zone. Ternary reactions that promote the recombination of radicals are not observed in this low-pressure system. Indeed, it is the suppression of ternary reactions that results in a greatly extended secondary reaction zone making H, O, and OH appear as products in the composition profiles. These data do indirectly support the idea that the inhibitor affects the H, O, and OH populations at maximum flame temperatures. H, O, and OH populations are observed to be in partial equilibrium at maximum flame temperatures, and inhibited adiabatic flames have reduced temperatures.

The calculated net reaction rate profiles show that the reactions of the inhibitor are not simple or limited to one region. The inhibitor decomposes/reacts and, along with its reaction and decomposition products, continues to be chemically active throughout the flame. At low temperatures, the inhibitor absorbs heat when it decomposes. It competes with the fuel and oxidizer in reactions with radicals (primarily H). The inhibitor related species also compete with the radicals in reaction with the fuel and tie up H atoms.

It is conjectured that an inhibited and uninhibited flame of the same heat loss (instead of at the same propagation velocity as studied here) would exhibit greater radical (H, O, OH) population reduction than observed here. Unfortunately, adiabaticity is not easily achieved in flat flame burner systems.

REFERENCES

1. Baulch, C. L., D. D. Drysdale, D. G. Horne, and A. C. Lloyd. Evaluated Kinetic Data for High Temperature Reactions. V. 1. Homogenous Gas Phase Reactions of the H_2-O_2 System. CRC Press, Cleveland, Ohio, 1972, 433 pp.

2. Baulch, D. L., D. D. Drysdale, J. Duxbury, and S. Grant. Evaluated Kinetic Data for High Temperature Reactions. V. 3, Homogeneous Gas Phase Reactions of the O_2-O_3 System, the CO-O_2-H_2 System and of Sulphur Containing Species. Butterworth (Publishers) Inc., London, England, 1978, 593 pp.

3. Biordi, J. C., C. P. Lazzara, and J. F. Papp. Flame Structure Studies of CF_3Br Inhibited Methane Flames. 14th Symp. (Internat.) on Combustion, Combustion Inst., Pittsburgh, Pa., 1973, pp. 367-381.

4. _____. Chemical Flame Inhibition Using Molecular Beam Mass Spectrometry Bromotrifluoromethane in Low-Pressure Methane-Oxygen-Argon Flames. BuMines RI 7723, 1973, 39 pp.

5. _____. Molecular Beam Mass Spectrometry Applied to Determining the Kinetics of Reactions in Flames. I. Empirical Characterization of Flame Perturbation by Molecular Beam Sampling Probes. Combustion and Flame, v. 23, 1974, pp. 73-82.

6. _____. Chemical Flame Inhibition Using Molecular Beam Mass Spectrometry. Reaction Rates and Mechanisms in a 0.3 Percent CF_3Br Inhibited Methane Flame. BuMines RI 8029, 1975, 42 pp.

7. _____. Flame Structure Studies of CF_3Br-Inhibited Methane Flames. II. Kinetics and Mechanisms. 15th Symp. (Internat.) on Combustion, Tokyo, Japan, Aug. 25-31, 1974, Combustion Inst., Pittsburgh, Pa., 1975, pp. 917-932.

8. _____. On the Inhibition of Low Pressure Quenched Flames by CF_3Br. Combustion and Flame, v. 24, 1975, pp. 401-403.

9. _____. Mass Spectrometric Observation of Difluorocarbene and Its Reactions in Inhibited Methane Flames. J. Phys. Chem., v. 80, 1976, pp. 1042-1048.

10. _____. Molecular Beam Mass Spectrometry Applied To Determine the Kinetics of Reactions in Flames. II. A Critique of Rate Coefficient Determinations. Combustion and Flame, v. 26, 1976, pp. 57-76.

11. _____. Flame Structure Studies of CF_3Br-Inhibited Methane Flames. 3. The Effect of 1% CF_3Br on Composition, Rate Constants, and Net Reaction Rates. J. Phys. Chem., v. 81, No. 12, 1977, pp. 1139-1145.

12. Biordi, J. C., C. P. Lazzara, and J. F. Papp. Chemical Flame Inhibition Using Molecular Beam Mass Spectrometry. An Examination of the Partial Equilibrium Hypothesis and Radical Recombination in 1/20 Atm Methane Flames. BuMines RI 8222, 1977, 33 pp.

13. _____. Flame Structure Studies of Bromotrifluoromethane-Inhibited Methane Flames. 4. Reactions of Inhibitor-Related Species in Flames Containing Initially 1.1% Bromotrifluoromethane. J. Phys. Chem., v. 82, 1978, pp. 125-132.

14. _____. Chemical Flame Inhibition Using Molecular Beam Mass Spectrometry. Reaction Rates and Mechanisms in a Methane Flame Inhibited by 1.1% CF_3Br. BuMines RI 8307, 1978, 43 pp.

15. Bradley, D., and A. G. Entwistle. Determination of the Emissivity, for Total Radiation, of Small Diameter Platinum-10% Rhodium Wires in the Temperature Range 600-1,450° C. Brit. J. Applied Phys., v. 12, 1961, pp. 708-711.

16. Ferguson, C. R., and J. C. Keck. Stand-Off Distances on a Flat Flame Burner. Combustion and Flame, v. 34, 1979, pp. 85-98.

17. Fristrom, R. M., and A. A. Westenberg. Flame Structure, McGraw-Hill Book Co., New York, 1965, 424 pp.

18. Gordon, S., and B. J. McBride. Computer Program for Calculation of Complex Chemical Equilibrium Composition, Rocket Performance, Incident and Reflected Shocks, and Chapman-Jouget Detonations. NASA SP-273, 1971, 26 pp.

19. Hays, K. F., and W. E. Kaskan. Inhibition by CH_3Br of CH_4/Air Flames Stabilized on a Porous Plug Burner. Combustion and Flame, v. 24, 1975, pp. 405-407.

20. Herron, J. T. An Evaluation of Rate Data for the Reactions of Atomic Oxygen ($O\,^3P$) with Methane and Ethane. Internat. J. Chem. Kinetics, v. 1, 1969, pp. 527-539.

21. Hilsenrath, J., C. W. Bechett, W. Benedict, L. Fano, H. G. Hoge, J. Masi, R. L. Nuttall, Y. Toulkian, and H. W. Woolley. Tables of Thermal Properties of Gases. NBS Circ. 564, 1955, pp. 128-129.

22. Iya, K. Sridhar, S. Wollowitz, and W. E. Kaskan. The Measure of Inhibition of Quenched Premixed Flames. Combustion and Flame, v. 22, 1974, pp. 415-417.

23. Iya, K. S., S. Wollowitz, and W. E. Kaskan. The Mechanism of Flame Inhibition by Sodium Salts. 15th Symp. (Internat.) on Combustion, Tokyo, Japan, Aug. 25-31, 1974, Combustion Inst., Pittsburgh, Pa., 1975, pp. 329-336.

24. Kaskan, W. E. The Dependence of Flame Temperature on Mass Burning Velocity. 6th Symp. (Internat.) on Combustion, Combustion Inst., Pittsburgh, Pa., 1957 pp. 134-143.

25. Kaskan, W. E., and J. J. Reuther. Limiting Equivalence Ratio, Dissociation, and Self-Inhibition in Premixed, Quenched, Fuel-Rich Hydrocarbon/Air Flames. 16th Symp. (Internat.) on Combustion, Mass. Inst. Technol, Aug. 15-21, 1976, Combustion Inst., Pittsburgh, Pa., 1977, pp. 1083-1095.

26. Kondratiev, V. N. Rate Constants of Gas Phase Reactions. Academy of Sciences of the U.S.S.R., Order-of-Lenin Institute of Physics. National Technical Information Service, Springfield, Va., 1972, NTIS Com-72-10014.

27. Lazzara, C. P., J. C. Biordi, and J. F. Papp. Concentration Profiles for Radical Species in a Methane-Oxygen-Argon Flame. Combustion and Flame, v. 21, 1973, pp. 371-382.

28. _____. Radical Species Profiles for a Methane-Oxygen-Argon Flame. BuMines RI 7766, 1973, 10 pp.

29. LeMoan, G., and M. Chaigneau. Analyses Des Composes Formes Au Cours De La Decomposition Thermique Des Fluoroalcanes Cas Du Dibromodifluoro-methane (CF_2Br_2). [(Analyses of Compounds Formed During Thermal Decomposition of Fluoroalkanes. Dibromodifuoromethane (CF_2Br_2.)] Ann. Fals. Exp. Chim., v. 67, 1974, pp. 341-350.

30. Papp, J. F., C. P. Lazzara, and J. C. Biordi. Chemical Flame Inhibition Using Molecular Beam Mass Spectrometry. Computational Methods for Analyzing Flame Microstructure. BuMines RI 8019, 1975, 90 pp.

31. Peeters, J., and G. Mahnen. Reaction Mechanisms and Rate Constants of Elementary Steps in Methane-Oxygen Flames. 14th Symp. (Internat.) on Combustion, Combustion Inst., Pittsburgh, Pa., 1973, pp. 133-146.

32. Powell, R. L., W. J. Hall, G. H. Hyink, L. L. Sparks, G. W. Burns, M. G. Scroger, and H. H. Plumb. Thermocouple Reference Tables based on the IPTS-68, NBS MN-125, 1974, 401 pp.

33. Reuther, J. J. Comments on Chemical and Physical Inhibition of Quenched and Adiabatic Flames, Pres. at The Eastern Section Meeting of the Combustion Institute, November, 1977, East Hartford, Conn. Available upon request from J. J. Reuther, The Pennsylvania State University, University Park, Pa.

34. Savitzky, A., and M. J. E. Golay. Smoothing and Differentiation of Data by Simplified Least Squares Procedure. Anal. Chem. v. 36, 1964, pp. 1627-39.

35. Steiner, J., Y. Termonia, and J. Deltour. Comments on Smoothing and Differentiation of Data by Simplified Least Square Procedure. Anal. Chem. v. 44, 1972, pp. 1906-1909.

36. Walton, J. C. Photolysis of Dibromodifluoromethane at 265 nm. Chem. Soc., Farday Trans. I, v. 68, 1972, pp. 1559-1565.

37. Wilson, W. E., J. T. O'Donovan, and R. M. Fristrom. Flame Inhibition by Halogen Compounds. 12th Symp. (Internat.) on Combustion, Combustion Inst., Pittsburgh, Pa., 1969, pp. 929-942.

38. Yudin, B. F., and G. A. Khachkuruzov. Heats of Formation of Halogen Derivatives of Methane. Tr. Gosudarstvennyi Inst. Prikladnoi Khimi, v. 42, 1959, pp. 137-157.

39. Zabetakis, M. G. Flammability Characteristics of Combustible Gases and Vapors. BuMines Bull. 627, 1965, 121 pp.

☆U.S. GOVERNMENT PRINTING OFFICE: 1981-703-002/60 INT.-BU.OF MINES,PGH.,PA. 25407